OPEN

PRS GLOBAL OPEN

ORIGINAL ARTICLE
Reconstructive

Technical Challenges in "Micro" Lymph Node Identification during Vascularized Submental Lymph Node Flap Harvesting

Nutcha Yodrabum, MD*
Krittayot Patchanee, MD†
Thanaphorn Oonjitti, MD*†
Parkpoom Piyaman, MD†

Background: The outcome of autologous lymph node (LN) transfer has depended on the number of LNs in the donor site. Unknown accuracy of the LN counting method has thrown some doubts on the reliability of the previous statistics. This study aimed to assess the accuracy of naked eye (NK) and stereo microscopy (SM) as tools for LN count.

Methods: In total, 40 vascularized submental LN flaps were harvested from 23 fresh cadavers. The colored polymer was injected into the external carotid arteries before the harvest. LNs in each flap were counted by NK, SM, and histology in sequential order.

Results: An estimated 175 LNs were confirmed, 4.4 ± 1.8 per flap. NK sensitivity was 33.7% compared with that of SM at 63.5%. Both methods missed all micro-lymph nodes (micro-LNs), contributing to 5.1% (9 nodes) of all LNs. Non-LN structures (647 negative counts) were composed of fat lobules, salivary gland lobules, and muscle fibers. NK specificity was 98.0%, compared with that of SM at 96.1%. SM showed a higher false positive rate at 14.3%, compared with NK at 7.4%. False positive counts were located mostly in Ib sublevel.

Conclusions: NK and SM are imperfect tools for LN count due to poor sensitivity. If the method needs to be applied, points of considerations are (1) undetectable micro-LNs, (2) interposition of LNs with the digastric muscle and submandibular salivary gland, (3) confusion of LNs with lobules of salivary gland supplied by glandular artery or fat lobules supplied by lobular artery. *(Plast Reconstr Surg Glob Open 2020;8:e3330; doi: 10.1097/GOX.0000000000003330; Published online 18 December 2020.)*

INTRODUCTION

There is no gold standard treatment for lymphedema. Vascularized lymph node transfer (VLNT) is the most recent development, which becomes a new horizon in the physiologic treatment.[1–6] Lymph nodes (LNs) from various sites have been selected: groin,[7] submental,[8] supraclavicular,[9] thoracodorsal,[10] lateral thoracic,[11] internal mammary,[12] deep inferior epigastric,[13] lateral intercostal artery,[14] gastroepiploic,[15,16] jejunal mesentery,[17,18] mesoappendix,[19,20] and ileocecal area.[21] The systematic reviews and meta-analysis have shown many satisfactory results.[22–24] The mechanism of vascularized LN flap is still unsettled. The possible explanations fall either into pumping mechanism theory[25–28] or lymphangiogenesis theory.[25,29–31] Fortunately, both theories are grounded in the existence of LNs in the flap. The significance of quantity of transferred LNs has been demonstrated in animal[32,33] and clinical studies.[34] Apart from that, the success of the treatment is also attributed to donor site morbidity and anatomic reliability.[34]

In search of the optimal donor site, various methods have been applied to detect LNs: surgical exploration with the naked eye (NK) or surgical exploration under operative microscope[8,35,36] and imaging studies.[35,37,38] However, little is known about the sensitivity and specificity of each of these methods. On top of that, a study of gastroepiploic LN flap[39] has revisited micro-lymph nodes (micro-LNs) defined by the diameter <1.5 mm.[40] A significant proportion of micro-LNs along greater curvature (nodal station 4) has raised questions about distribution of them in other donor sites. Undetectability of micro-LNs also raised some

*From the *Division of Plastic and Reconstructive Surgery, Department of Surgery, Faculty of Medicine Siriraj Hospital, Mahidol University, Bangkok, Thailand; and †Department of Anatomy, Faculty of Medicine Siriraj Hospital, Mahidol University, Bangkok, Thailand.*

Received for publication July 13, 2020; accepted October 21, 2020.

Presented at the 10th Congress of World Society for Reconstructive Microsurgery (WSRM 2019), June 12–15, 2019, Bologna, Italy.

DOI: 10.1097/GOX.0000000000003330

Disclosure: *The authors have no financial interest to declare in relation to the content of this article.*

doubts on the accuracy of previous data derived from the NK and surgical stereo microscopy (SM).

MATERIALS AND METHODS

This study aimed to assess the accuracy of 2 LN counting methods: the NK and SM. Both methods were compared with histological observation (HIS) set as gold standard. The counting was conducted in submental LN flap due to a large number of LN41 and anatomic complexities. The latter involves marginal mandibular nerves, digastric muscle, platysma muscle, and submandibular gland, which requires extra care during flap harvest.[8,35,37]

Forty vascularized submental LN flaps were obtained from 23 fresh cadavers self-donated to the Department of Anatomy, Faculty of Medicine Siriraj Hospital, Mahidol University. Cadavers were of Thai nationality, with 10 being male and 13 being female specimens. The ages of these specimens ranged from 56 to 76 years. Exclusion criteria were (1) visible cranial and cervical deformity, (2) medical history of lymphatic diseases involving the head and neck, and (3) visible surgical wound to the cervical Ia/Ib sublevel. The procedure was approved by Siriraj Institutional Review Board (SiRB) with protocol number 366/2561(Exempted).

Arterial injections were performed according to Piyaman et al.[42] In brief, external carotid arteries of both sides were cannulated, irrigated with 0.9% saline solution and injected with red polyacrylamide solution. The amount of injected solution was 80 ml per vessel, 160 ml per head. Flap design was elliptical skin paddle, where longitudinal axis ran from mental protuberance (gnathion) to angle of mandible (gonion). Medial curve was demarcated roughly by both bellies of digastric muscle, while lateral curve by inferior mandibular border. The dissection included (1) the anterior belly of digastric muscles, (2) the entire submental artery, (3) the segment of facial artery from its origin to mandibular border, and (4) the superficial part of the submandibular gland. Once the flaps were removed, they were fixed in 10% formalin and then sliced to 2-mm thickness. All slices were subjected to routine histological process: dehydration, paraffin embedding, and H&E staining. Each paraffin block representing a slice of a flap was cut into 5–200 microscopic slides for accurate LN count.

Counting the Lymph Nodes

LN counts were performed by 3 methods: NK, SM (equivalent to operative microscope), and HIS (Fig. 1). NK count was conducted during flap dissection by the qualified plastic surgeon (NY). Next, the anatomist (PP) fixed the harvested flap in 10% formalin and performed SM count at 10×–20× magnification. Then, the flaps were processes into series of H&E microscopic slides. The anatomist performed HIS count by tracing the slides. HIS was set as definite LN identification, a "gold standard" method against which accuracy of NK and SM count would be tested. Identification criteria for LNs were based on morphology; these were the presence of capsule, cortex, medulla capsular arteries, and hilar arteries[43] (Fig. 2).

The counting was recorded as positive once LN was presented. Each node was counted only once; therefore, true positive counts would be matched with the number of confirmed nodes. On the other hand, a negative count was recorded once the node becomes absent in a finite area. The area covering 1 negative count was a 2-mm-thick slice of the flap. Each slice was subsequently processed into a paraffin block for serial histological sectioning and HIS count.

Grouping the Lymph Nodes (Micro-, Meso-, Macro-)

The LNs were classified by diameter into 3 groups. Firstly, micro-lymph node (micro-LN) had a diameter of <1.5 mm.[40] To complete the classification, 2 new terms were introduced: meso-lymph node (meso-LN) and macro-lymph node (macro-LN). Meso-LNs had a diameter ranging from 1.5 mm to <5.0 mm. Lastly, macro-LNs had a diameter of 5.0 mm and larger. LNs were also classified by location into cervical sublevel Ia and Ib. This study assigned the lateral (posterior) border of the anterior belly of digastric muscles (ABDM) as the demarcation line between Ia and Ib sublevel. According to this demarcation, Ib nodes were categorically located lateral to anterior belly of digastric muscle, whereas Ia nodes were further subdivided into medial, superficial, and deep zones relative to the muscle.

Statistical Analysis

The number and the size of LNs in each submental LN flap were counted by 3 methods: (1) by using surgical exploration with the NK, (2) by using a 10× stereo microscope (SM), and (3) by HIS under a light microscope. The data were represented by arithmetic mean ± SD. For accuracy test, the results from the first 2 methods were compared with histological observation. The accuracy was represented by (1) sensitivity, (2) specificity, (3) false positive rate, and (4) false negative rate. The LNs were further classified by size (micro-, meso-, macro-) and neck sublevel (Ia, Ib). The subgroup analyses were performed by comparing the accuracy between subgroups.

RESULTS

From 40 flaps, 175 LNs were confirmed by HIS (+ + +, - + +, + - +, and - - + in Fig. 3). The average number was 4.4 ± 1.8 nodes per flap. The average LN size was measured 4.4 ± 2.2 mm, ranging from 1.0 to 10.7 mm (Table 1). LNs were classified by size into 9 micro-LNs (5.1%), 113 meso-LNs (64.6%), and 50 macro-LNs (28.6%) (Table 2). LNs were classified by location into 52 nodes in Ia (29.7%) and 123 nodes in Ib (70.3%). All Ib nodes, by our definition, were located lateral to the ABDM and relatively close to the submandibular gland (SMG). On the other hand, Ia nodes were further subdivided by topographic relationship with the ABDM into 30 superficial nodes, 10 deep nodes, and 15 medial nodes.

Naked eye (NK) detected 1.9 ± 1.4 nodes per flap (Table 1), yielding 33.7% sensitivity (Table 3 and +++, +-+ in Fig. 3). Of all the nodes detected by NK, the size ranged from 1.7 mm to 10.9 mm, 5.3 ± 2.3 mm by average (Table 1).

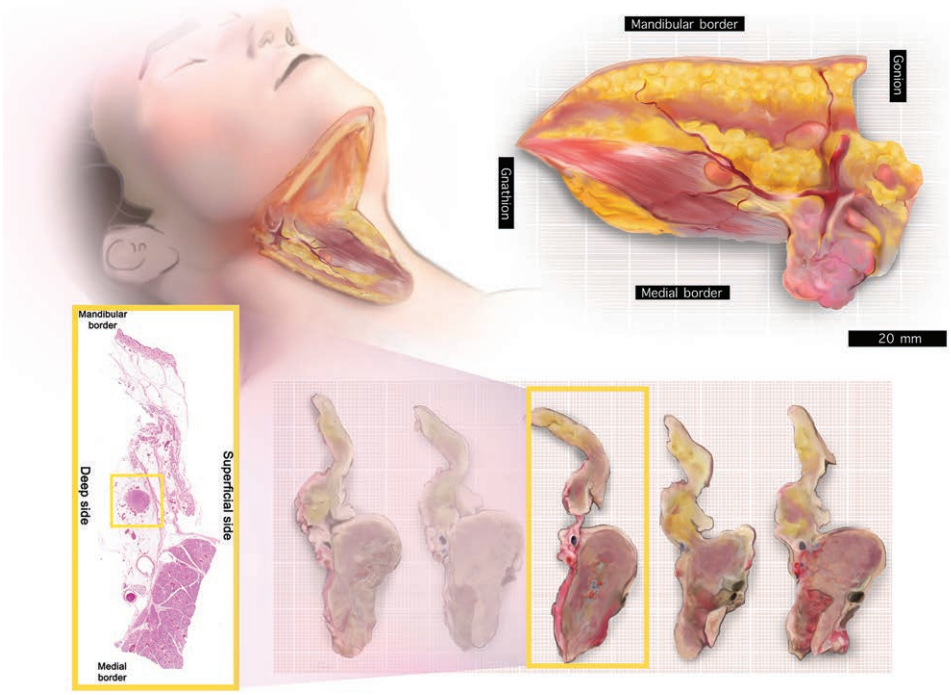

Fig. 1. Schematic drawings showing 3 steps of counting methods. A, LN count under NK during flap dissection; B, LN count under ×10–×20 SM was performed after formalin fixation (equivalent to operative microscope); and C, the entire flap were sliced at 2-mm thickness and subjected to histological processes and counted under a "gold standard" histology.

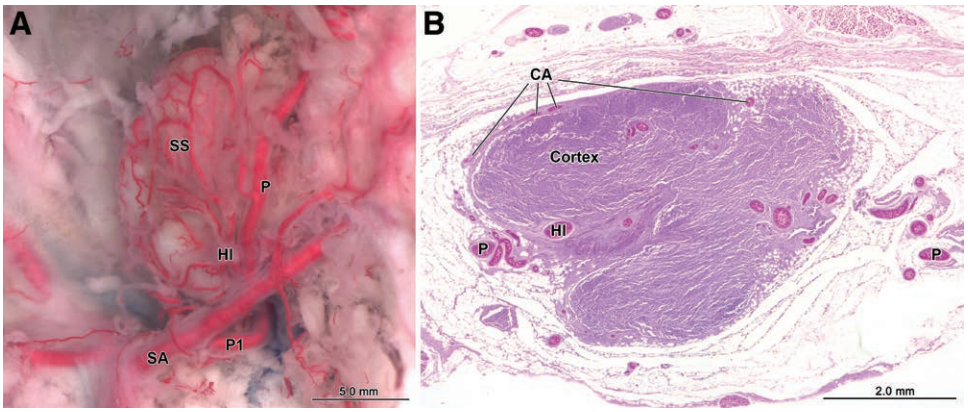

Fig. 2. Attributes of true LNs. The pictures present the generic form of LN. A, A photograph showing the submental LN supply by submental artery (SA) via submental perforator (P). The P branches from the SA at P1. Afterward, it branches to the hilar artery (HI) and capsular artery (CA) before reaching the skin (P). The plexus of CA enfolds the LN. B, A micrograph, which is comparable to the left picture, is composed of P, HI, capsule, cortex, and CA.

Subgroup analysis showed that the sensitivities increased with size, from 0% for the micro-LN, 27.4% for the meso-LN to 54.0% for the micro-LN (Table 2). Subgroup analysis also shows different sensitivities between 2 sublevels; 21.2% in sub-level Ia and 39.0% in Ib sub-level (Table 3).

Stereo microscopy (SM) detected 3.4 ± 1.4 nodes per flap (Table 1), yielding 63.5% sensitivity (Table 3 and +++, -++ in Fig. 3). Of all the nodes detected by SM, the size ranged from 1.6 to 10.9 mm, 5.0 ± 2.1 mm by average (Table 1). Sensitivities increased with size, from 0% for the micro-LN, 56.6% for the meso-LN to 92.0% for the macro-LN (Table 2). Sensitivities varied by location, from 50.0 % in Ia sublevel to 69.1% in Ib (Table 3).

Non-LN structures, confirmed by HIS, detected 647 true negative counts in total (+ + -, - + -, + - - and - - - in Fig. 3). Among these, NK detected 634 true negative counts, yielding 98.0% specificity. SM detected 622 true negative counts, yielding 96.1% specificity (Table 3).

There were totally 30 false positive counts by any methods (+ + -, - + -, and + - - in Fig. 3). Most of them, 26 counts,

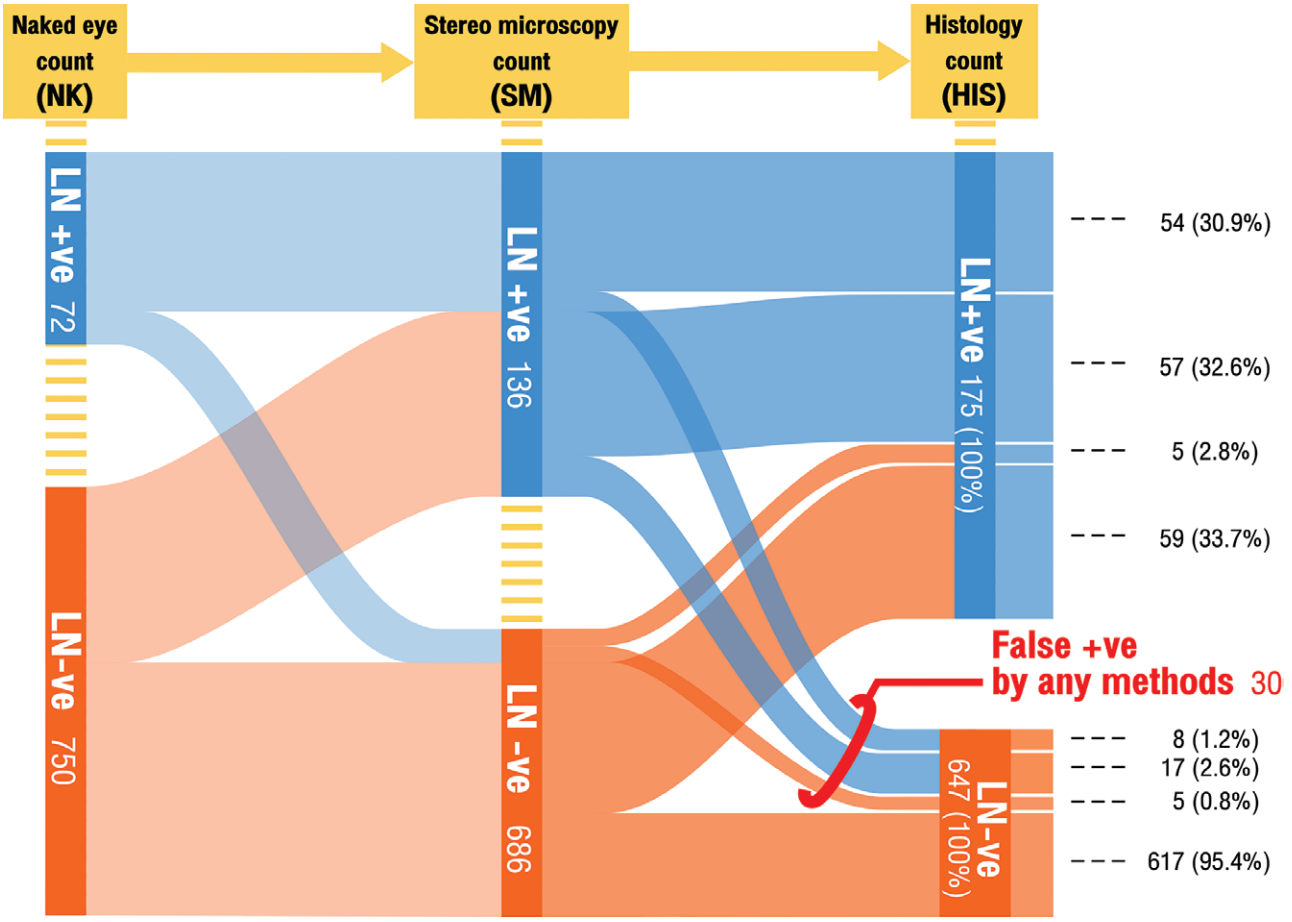

Fig. 3. A Sankey diagram showing the flow of LN counting process from the NK, SM to HIS, which are represented in 3 columns. From the left: the NK column. The NK count divides all structures into LNs (LN +ve) and non-LN structures (LN –ve), which are represented by 2 horizontal bands. When count is proceeded, the bands are shuffled again and again into the final horizontal bands of (LN +ve) and (LN –ve) at the HIS column. The data are represented in short by 3 characters of + or –, for each of which represents the result from NK, SM, and HIS, respectively. All confirmed (positive) LNs are (+++), (-++), (+-+), (--+) combined, 175 nodes in total. All non-LN structures are (++-), (-+-), (+--), (---) combined, 647 counts in total. False positive nodes by any method (NK or SM) are (++-), (+--), (-+-) combined, 30 counts in total.

Table 1. Size and Number of LNs Classified by Detection (Counting) Methods

	Detection methods		
	NK	SM	HIS
No. LN per flap	1.9 ± 1.4	3.4 ± 1.4	4.4 ± 1.8
Size of LN (mm)	5.3 ± 2.3 [range, 1.7–10.9]	5.0 ± 2.1 [range, 1.6–10.9]	4.4 ± 2.2 [range, 1.0–10.7]

Data are represented by mean ± SD unless otherwise specified.

Table 2. Sensitivity of NK and SM in LN Detection Classified by Size (Subgroup Analysis)

	Overall	Micro-LN (<1.5 mm)	Meso-LN (≥1.5, <5 mm)	Macro-LN (≥5 mm)
No. LN (%)	175 (100)	9 (5.1)	113 (64.6)	50 (28.6)
NK sensitivity	33.7	0	27.4	54.0
SM sensitivity	63.4	0	56.6	92.0

Table 3. Accuracy of NK and SM in LN Detection Classified by Cervical Sublevel (Subgroup Analysis)

	Detection Methods	Cervical Sublevels		
		Ia + Ib	Ia	Ib
Sensitivity (%)	NK	33.7	21.2	39.0
	SM	63.5	50.0	69.1
Specificity (%)	NK	98.0	100.0	96.3
	SM	96.1	98.7	93.9
False positive rate (%)	NK	7.4	0.0	10.6
	SM	14.3	7.7	17.1
False negative rate (%)	NK	17.9	13.7	21.6
	SM	9.9	8.7	11.0

were located in Ib sublevel. Accordingly, Ib sublevel had a higher false positive rate than Ia. The causes of false positivity included fat, SMG, muscle (Fig. 4), and double counting. The latter occurred when single extensive LNs were mistaken as 2 separate nodes. False positivity was categorized into 3 scenarios (Fig. 5): (1) double falsified, (2) corrected-by-SM, and (3) corrupted-by-SM. Double falsified

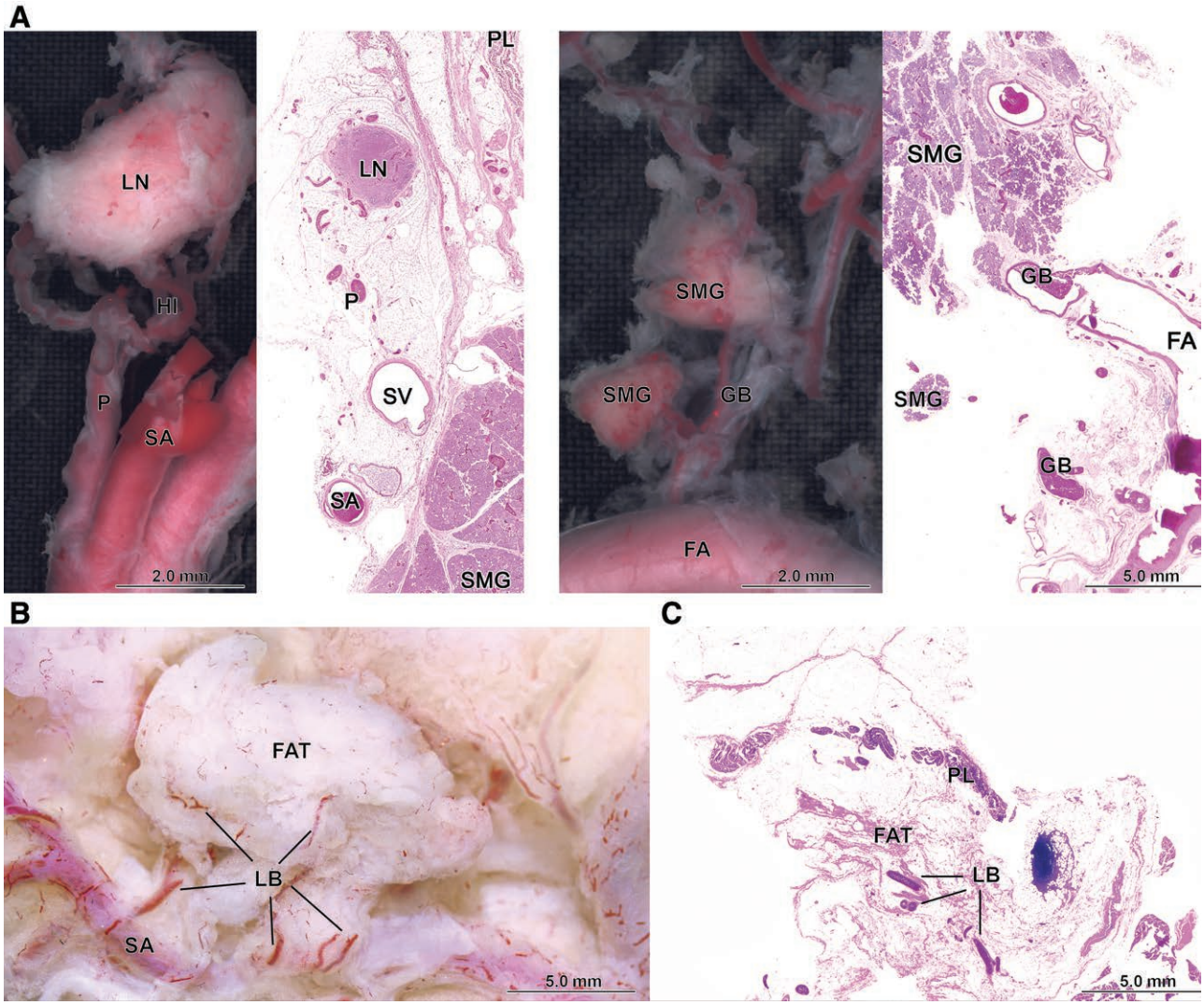

Fig. 4. Causes of the false positivity. The photographs and the micrographs demonstrate the same structures of the potential false positive. The LN, the SMG, and the fat lobule are compared. A, The submental LN is supplied by the submental submental artery (SA) via the submental perforator (P) and hilar artery (HI). B, The SMG is often misled as an LN. It receives blood supply from the facial artery (FA) via glandular branch (GB). C, It shows fat lobule (FAT), which receives blood supply from the SA via the lobular branch (LB). PL, platysma muscle.

scenario, 8 counts, occurred when both NK and SM mistook fat or SMG for the LN. The corrected-by-SM scenario, 5 counts, occurred when NK mistook fat or SMG for the LN at first, but the structures were identified correctly later by SM. Lastly, the corrupted-by-SM scenario, 17 counts, occurred when non-LN structures were correctly identified by NK at first, but they were counted as the LN by SM later.

DISCUSSION

LN count under the NK (the conventional method) shows a very low sensitivity. The method missed two-thirds of LNs of all size and failed to detect any micro-LN smaller than 1.5 mm. The sensitivity was still inadequately low to count the node larger than 5 mm by missing half of them. Therefore, the naked eye is not suitable for LN detection. The result is supported by Okamura's study,[44] which showed only 13.8% accuracy of macroscopic (NK) detection of LNs under 5 mm. However, an average detectable size of metastatic LN in stomach cancer was reduced to 4.06 ± 0. 95 mm.[45] The reduction may be due to harder consistency of metastatic LNs, making LN detection easier.

SM showed average detectable size at 5.0 mm, similar to NK at 5.3 mm. SM also failed to detect any micro-LN as well as NK. Nevertheless, the overall SM sensitivity is twice as much as NK and is exceptionally high for LNs > 5.0 mm. SM could detected 3.4 ± 1.4 nodes per flap. The number was consistent with the surgical exploration in the previous studies[8,35,37] (Table 4).

Lower sensitivity in Ia sublevel compared with Ib sublevel was probably due to interposition of Ia LN with the ABDM. In the attempt to harvest Ia nodes, the surgeon has to choose how to approach the ABDM. Whether the approach is proceeded on the superficial or deep aspect

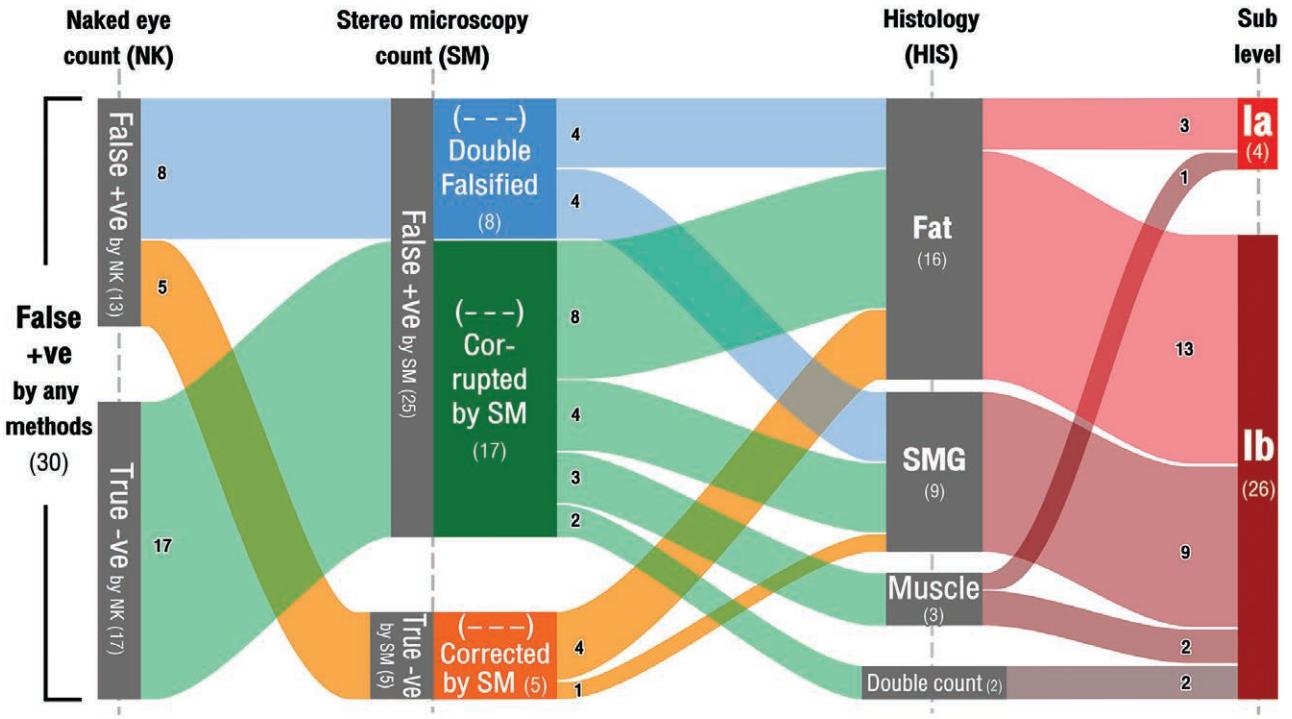

Fig. 5. Sankey diagram of false positivity. Sankey diagram represents how all false positive structures flowing through the counting process from left to right. The first 3 columns represent 3 counting methods, whereas the last column represents the locations of each structure that are classified by cervical sublevels. The horizontal bands reflect how each structure is counted, re-counted, and finally identified as non-LN structures (eg, fat, SMG, muscle). Most of the false positive counts were fat and submandibular glands, which are mostly located in the Ib sublevel. The SM causes more false positivity than NK. Three false positive scenarios were double falsified (++-), corrupted by SM (-+-), and corrected by SM (+--) scenarios.

Table 4. Previous Clinical and Anatomical Studies on Submental LN Flap

Study	Study Type	Number of Flaps	No. LN by Method of Study		
			Imaging	NK or SM	HIS
Cheng 2012[8]	Anatomy	12	—	2.3 ± 0.8	3.3 ± 1.5
	Clinical	6	—	—	—
Patel 2015[36]	Clinical	12	—	—	—
Tzou 2017[35]	Anatomy	18	3.2 ± 1.0 (US)	3.0 ± 0.6	—
Asuncion 2018[37]	Clinical	19	3.2 ± 1.1 (US) 5.2 ± 1.9 (CT) 7.2 ± 2.4 (MRI)	3.1 ± 0.6	—
Gustafsson 2018[34]	Clinical	35	3.9 ± 1.9 (US)	—	—
Nonomura 2018[46]	Anatomy	4	—	2—3	—
	Clinical	6	—	2—3	—
Paulus 2020[38]	Clinical	104	5.3 ± 2.0 (CTA)	—	—

Data are reported as mean ± SD, unless otherwise specified.
CT, computed tomography; CTA, computed tomography angiography; MRI, magnetic resonance imaging; US, ultrasonography.

of the ABDM, the harvest would inevitably miss the node located on the opposite side of the muscle. The superficial approach seems preferable due to the larger number of the node located on superficial side. However, one should be aware that these superficial nodes usually receive arterial supply from the deep aspect of the muscle.[42]

Lower specificity in Ib sublevel compared with Ia was probably caused by the confusion among LNs, fat lobules, SMG lobules, and the muscle (Fig. 4). Their morphologies seem straightforwardly different; however, the pattern of the vasculatures complicated the identification. Submental artery supplies Ia/Ib sublevel as multiple minute branches. Hilar branches supplying the LN may come directly from the submental artery; the direct route, or indirectly from submental perforator; sharing route pattern.[42] In case of direct route, hilar branch may be confused with the glandular branch piercing capsule of salivary gland or even muscular branch piercing the muscular fascia. On the other case, hilar artery may run in the sharing route pattern, mimicking lobular branches from the perforator to fatty tissue. Most of the confusions occurred during SM counting despite higher visual resolution compared with the NK. Recently, a study has developed a new harvest technique that claimed to obtain more LNs near SMG.[46] Another study has shown that LNs located near SMG are supplied by glandular

branch from the facial artery.[47] Unfortunately, abovementioned studies did not include histological observation. According to our study, identification of LNs near SMG should be conducted with great caution and not to be confused with glandular branches supplying the lobule of salivary gland.

Accuracy of Imaging Studies

Compared with previous imaging studies (Table 4), higher LN counts were reported from MRI (7.2 ± 2.4),[37] CT studies (5.2 ± 1.9),[37] and CT-angiography (CTA) (5.3 ± 2.0).[38] On the other hand, ultrasound (US) count showed a significantly lower number (3.2 ± 1.0 and 3.2 ± 1.1).[35,37] The larger number from the MRI study seems to be the benefit from more extensive count, including jugulodigastric node in IIa sublevel and the additional submandibular node nestled deep to the submandibular gland. Both LN groups are supplied by facial arteries and still relevant to the flap harvest.

Even though the US-based method is operator-dependent, which leads to lower sensitivity than other imagings, the ultrasonography can provide specificity equal to or higher than that of CT48 and MRI.[49] Additionally, the method is more suitable for intraoperative usage.[50] Recent developments in the resolution[51] and application of color, power doppler, and 3D modalities[52] have increased advantage of this method for LN detection.

Roles of ICG Lymphography

ICG (indocyanine green dye) is suitable for real time and intraoperative evaluation of lymphatic drainage.[53] ICG lymphography has been applied for LN detection in sentinel LN biopsy for 2 decades.[54] Later, the method has been incorporated into lymphedema management as a tool for diagnosis and treatment monitoring. The method has visualized the basic mechanism of VLNT[26,28] and improved LN selection called reverse lymphatic mapping.[55] The selection has been developed to prevent iatrogenic lymphedema of donor site in axillary and inguinal VLNT. Focusing on submental VLNT, the clinical application of ICG is still limited. The LN detections have been conducted preoperatively by magnetic resonance imaging,[37] computed tomography,[37] computed tomography angiography,[38] or ultrasonography.[34,37] The reverse lymphatic mapping has not been applied to the area yet probably due to zero incidence of iatrogenic lymphedema.[56] The lymphatic vasculature in the area has been established by a similar method of lymphangiography.[57,58] Hence, the focus of recent anatomic studies was on blood vasculature of the LNs. ICG lymphography, nevertheless, should be incorporated in future anatomic studies for 2 purposes. Firstly, accuracy of the ICG method for LN detection could be tested. Secondly, the complete vasculature of the area (artery, vein, and lymphatic) could be elaborated.

Micro-lymph Node: Detect the Undetectable

A peri-gastric LN study[40] has introduced the term "micro-lymph node" describing the node < 1.5 mm. Undetectability of this LN group had raised a concern in the field of gastric cancer study, contributing to 36% of all LNs in Japanese station No. 4 (greater curvature nodes). In 2018, gastroepiploic vascularized LN flap has been introduced as lymphedema treatment and the micro-LN has been re-investigated.[39] According to our data, Ia/Ib sublevel contains a much lesser proportion of micro-LNs compared with gastroepiploic LNs (4% versus 36%). Ia/Ib LNs are more likely to be activated by immune reaction and subsequently become hyperplasia. The wider range of activation could come from upper gastrointestinal tract, upper respiratory tract, and the others in the head and neck areas.

Recently, lymph vessel-only vascularized transfer, as known as lymphadiposal flaps, has been demonstrated with favorable outcome.[59,60] The possible mechanism is relied on pumping of healthy lymphatic vessels of donor site to drain fluid into the vein in recipient site. In case of superficial circumflex iliac artery perforator flap (SCIP) as a donor site, the real mechanism is in doubt. The existence of micro-LN in SCIP has never been proved; thus, undetectable node may play hidden function, as described in "lymph node" flap. A further investigation into micro-LN in SCIP area is highly recommended.

Limitations of This Study

Firstly, this study was conducted in fresh cadavers, some of which were proceeded after another surgical workshop. In this case, decomposition certainly complicated differentiation of LNs from the surroundings. The latter was likely to lower the actual accuracy of the NK and SM, to some degree. Secondly, despite a prominent advantage of histology, implementing this method for LN count requires a lot of time and manpower. In the future, incorporation of artificial intelligence with the HIS or SM observation may shorten the study process.

Secondly, this study did not include lymphatic vasculature of the flap. The ICG lymphography or lymphangiography should be incorporated to the future anatomic study to complete the vasculature of the area. Additionally, the accuracy of the ICG method for LN detection could be tested.

CONCLUSIONS

Due to false positivity of NK and SM, the identification of the LN during the flap harvest should be performed with care. The tracing of hilar artery to the LNs may be misled to either glandular branch (artery) supplying lobule of salivary glands or lobular artery supplying fat lobule. Due to the low sensitivity of NK and SM, the pre-operative imaging modalities (ultrasonography, CT, CTA, or MRI) are advisable. We do not recommend harvesting the flap as large as possible to get the undetectable nodes. The extension of the flap into Ia sublevel, if necessary, should include submental artery and hilar branches, which are usually located deep (superior) to the digastric anterior belly.[42] On research perspective, the future study on LN distribution should incorporate histology or imagings to increase the accuracy of the data.

Parkpoom Piyaman, MD
Department of Anatomy
Faculty of Medicine Siriraj Hospital
Mahidol University
2 Wanglang Road
Bangkok Noi District
Bangkok, Thailand
E-mail: ppiyaman@gmail.com

ACKNOWLEDGMENTS

We thank Suphalerk Lohasammakul, Warit Chongkolwatana, Phattarapong Predapramote, and Kittipich Sangkamard (Department of Anatomy, Faculty of Medicine Siriraj Hospital, Mahidol University) for their excellent surgical skill. We also thank all staffs at the Micro technique Unit, Department of Anatomy for the painstaking production of serial microscopic sections, and Chanagun Tounkhrua for industrious tracing and identification of all LNs. Finally, we are grateful to Supharak Khongchu (Research Department, Faculty of Medicine Siriraj Hospital, Mahidol University) for data analysis.

REFERENCES

1. Pappalardo M, Patel K, Cheng MH. Vascularized lymph node transfer for treatment of extremity lymphedema: an overview of current controversies regarding donor sites, recipient sites and outcomes. *J Surg Oncol*. 2018;117:1420–1431.
2. Ito R, Suami H. Overview of lymph node transfer for lymphedema treatment. *Plast Reconstr Surg*. 2014;134:548–556.
3. Schaverien MV, Aldrich MB. New and emerging treatments for lymphedema. *Semin Plast Surg*. 2018;32:48–52.
4. Schaverien MV, Coroneos CJ. Surgical treatment of lymphedema. *Plast Reconstr Surg*. 2019;144:738–758.
5. Scaglioni MF, Arvanitakis M, Chen YC, et al. Comprehensive review of vascularized lymph node transfers for lymphedema: outcomes and complications. *Microsurgery*. 2018;38:222–229.
6. Becker C. Autologous lymph node transfers. *J Reconstr Microsurg*. 2016;32:28–33.
7. Becker C, Assouad J, Riquet M, et al. Postmastectomy lymphedema: long-term results following microsurgical lymph node transplantation. *Ann Surg*. 2006;243:313–315.
8. Cheng MH, Huang JJ, Huang JJ, et al. A novel approach to the treatment of lower extremity lymphedema by transferring a vascularized submental lymph node flap to the ankle. *Gynecol Oncol*. 2012;126:93–98.
9. Althubaiti GA, Crosby MA, Chang DW. Vascularized supraclavicular lymph node transfer for lower extremity lymphedema treatment. *Plast Reconstr Surg*. 2013;131:133e–135e.
10. Dayan E, Smith ML, Sultan M, et al. Axillary lymph node transfer for the treatment of lymphedema: technique and case series. *Plast Reconstr Surg*. 2013;132(4S-1):86.
11. Barreiro GC, Baptista RR, Kasai KE, et al. Lymph fasciocutaneous lateral thoracic artery flap: anatomical study and clinical use. *J Reconstr Microsurg*. 2014;30:389–396.
12. Pannucci CJ, Gerety PA, Wang AR, et al. Feasibility of the internal mammary lymph node flap as a vascularized lymph node transfer: a cadaveric dissection study. *Microsurgery*. 2016;36:485–490.
13. Ochoa O, Metzner M, Theoharis C, et al. Deep inferior epigastric lymph node basin: Analysis of novel donor site for vascularized lymph node transfer among 10 consecutive patients. *Microsurgery*. 2019;39:215–220.
14. Kwak MD, Machens HG. The lateral intercostal artery perforator as an alternative donor vessel for free vascularized lymph node transplantation. *Arch Plast Surg*. 2018;45:275–279.
15. Egorov YS, Abalmasov KG, Ivanov VV, et al. Autotransplantation of the greater omentum in the treatment of chronic lymphedema. *Lymphology*. 1994;27:137–143.
16. Ciudad P, Kiranantawat K, Sapountzis S, et al. Right gastroepiploic lymph node flap. *Microsurgery*. 2015;35:496–497.
17. Coriddi M, Wee C, Meyerson J, et al. Vascularized jejunal mesenteric lymph node transfer: a novel surgical treatment for extremity lymphedema. *J Am Coll Surg*. 2017;225:650–657.
18. Schaverien MV, Hofstetter WL, Selber JC. Vascularized jejunal mesenteric lymph node transfer for lymphedema: a novel approach. *Plast Reconstr Surg*. 2018;141:468e–469e.
19. Ruter D, Chen W, Garza R III, et al. Mesoappendix as potential donor site for vascularized lymph node transfer: anatomic study. *J Surg Res*. 2018;230:143–147.
20. Ciudad P, Manrique OJ, Agko M, et al. Reply to comment on: ileocecal vascularized lymph node transfer for the treatment of extremity lymphedema: a case report. *Microsurgery*. 2018;38:723–724.
21. Ciudad P, Huang TC, Manrique OJ, et al. Expanding the applications of the combined transverse upper gracilis and profunda artery perforator (TUGPAP) flap for extensive defects. *Microsurgery*. 2019;39:316–325.
22. Basta MN, Gao LL, Wu LC. Operative treatment of peripheral lymphedema: a systematic meta-analysis of the efficacy and safety of lymphovenous microsurgery and tissue transplantation. *Plast Reconstr Surg*. 2014;133:905–913.
23. Ozturk CN, Ozturk C, Glasgow M, et al. Free vascularized lymph node transfer for treatment of lymphedema: a systematic evidence based review. *J Plast Reconstr Aesthet Surg*. 2016;69:1234–1247.
24. Carl HM, Walia G, Bello R, et al. Systematic review of the surgical treatment of extremity lymphedema. *J Reconstr Microsurg*. 2017;33:412–425.
25. Lin CH, Ali R, Chen SC, et al. Vascularized groin lymph node transfer using the wrist as a recipient site for management of postmastectomy upper extremity lymphedema. *Plast Reconstr Surg*. 2009;123:1265–1275.
26. Cheng MH, Huang JJ, Wu CW, et al. The mechanism of vascularized lymph node transfer for lymphedema: natural lymphaticovenous drainage. *Plast Reconstr Surg*. 2014;133:192e–198e.
27. Becker C, Vasile JV, Levine JL, et al. Microlymphatic surgery for the treatment of iatrogenic lymphedema. *Clin Plast Surg*. 2012;39:385–398.
28. Ito R, Zelken J, Yang CY, et al. Proposed pathway and mechanism of vascularized lymph node flaps. *Gynecol Oncol*. 2016;141:182–188.
29. Can J, Cai R, Li S, et al. Experimental study of lymph node autotransplantation in rats. *Chin Med J (Engl)*. 1998;111:239–241.
30. Shesol BF, Nakashima R, Alavi A, et al. Successful lymph node transplantation in rats, with restoration of lymphatic function. *Plast Reconstr Surg*. 1979;63:817–823.
31. Raju A, Chang DW. Vascularized lymph node transfer for treatment of lymphedema: a comprehensive literature review. *Ann Surg*. 2015;261:1013–1023.
32. Nguyen DH, Chou PY, Hsieh YH, et al. Quantity of lymph nodes correlates with improvement in lymphatic drainage in treatment of hind limb lymphedema with lymph node flap transfer in rats. *Microsurgery*. 2016;36:239–245.
33. Kwiecien GJ, Gharb BB, Tadisina KK, et al. Quantity of lymph nodes in the vascularized lymph node transfer influences its lymphaticovenous drainage. *J Reconstr Microsurg*. 2018;34:41–46.
34. Gustafsson J, Chu SY, Chan WH, et al. Correlation between quantity of transferred lymph nodes and outcome in vascularized submental lymph node flap transfer for lower limb lymphedema. *Plast Reconstr Surg*. 2018;142:1056–1063.
35. Tzou CH, Meng S, Ines T, et al. Surgical anatomy of the vascularized submental lymph node flap: anatomic study of correlation of submental artery perforators and quantity of submental lymph node. *J Surg Oncol*. 2017;115:54–59.

36. Patel KM, Lin CY, Cheng MH. A prospective evaluation of lymphedema-specific quality-of-life outcomes following vascularized lymph node transfer. *Ann Surg Oncol.* 2015;22:2424–2430.
37. Asuncion MO, Chu SY, Huang YL, et al. Accurate prediction of submental lymph nodes using magnetic resonance imaging for lymphedema surgery. *Plast Reconstr Surg Glob Open.* 2018;6:e1691.
38. Paulus VAA, Winters H, Hummelink S, et al. Submental flap for vascularized lymph node transfer; a CTA-based study on lymph node distribution. *J Surg Oncol.* 2020;122:1226–1231.
39. Agko M, Ciudad P, Chen HC. Histo-anatomical basis of the gastroepiploic vascularized lymph node flap: he overlooked "micro" lymph nodes. *J Plast Reconstr Aesthet Surg.* 2018;71:118–120.
40. Borchard F, Betz P. Number and size of perigastric lymph nodes in human adults without gastric cancer. *Surg Radiol Anat.* 1991;13:117–121.
41. Patel KM, Chu SY, Huang JJ, et al. Preplanning vascularized lymph node transfer with duplex ultrasonography: an evaluation of 3 donor sites. *Plast Reconstr Surg Glob Open.* 2014;2:e193.
42. Piyaman P, Patchanee K, Oonjitti T, et al. Surgical anatomy of vascularized submental lymph node flap: sharing arterial supply of lymph nodes with the skin and topographic relationship with anterior belly of digastric muscle. *J Surg Oncol.* 2020;121:144–152.
43. Miranda RN, Khoury JD, Medeiros LJ. Atlas of lymph node pathology. *Atlas of Anatomic Pathology.* New York, N.Y.: Springer;2013:xix.
44. Okamura T, Tsujitani S, Korenaga D, et al. Lymphadenectomy for cure in patients with early gastric cancer and lymph node metastasis. *Am J Surg.* 1988;155:476–480.
45. Candela FC, Urmacher C, Brennan MF. Comparison of the conventional method of lymph node staging with a comprehensive fat-clearing method for gastric adenocarcinoma. *Cancer.* 1990;66:1828–1832.
46. Nonomura H, Tan BK, Tan PWW, et al. A surgical approach to the harvest of the vascularized submandibular and submental lymph node flap: the "through-the-gland" dissection technique. *Ann Plast Surg.* 2018;80:432–437.
47. Tan PW, Goh T, Nonomura H, et al. Hilar vessels of the submandibular and upper jugular neck lymph nodes: anatomical study for vascularized lymph node transfer to extremity lymphedema. *Ann Plast Surg.* 2016;76:117–123.
48. Suh CH, Baek JH, Choi YJ, et al. Performance of CT in the preoperative diagnosis of cervical lymph node metastasis in patients with papillary thyroid cancer: a systematic review and meta-analysis. *AJNR Am J Neuroradiol.* Jan 2017;38:154–161.
49. Liu Z, Xun X, Wang Y, et al. MRI and ultrasonography detection of cervical lymph node metastases in differentiated thyroid carcinoma before reoperation. *Am J Transl Res.* 2014;6:147–154.
50. Tran BNN, Celestin AR, Lee BT, et al. Quantifying lymph nodes during lymph node transplantation: the role of intraoperative ultrasound. *Ann Plast Surg.* 2018;81:675–678.
51. Wunderbaldinger P. Problems and prospects of modern lymph node imaging. *Eur J Radiol.* 2006;58:325–337.
52. Ahuja AT, Ying M. Sonographic evaluation of cervical lymph nodes. *AJR Am J Roentgenol.* 2005;184:1691–1699.
53. Patel KM, Manrique O, Sosin M, et al. Lymphatic mapping and lymphedema surgery in the breast cancer patient. *Gland Surg.* 2015;4:244–256.
54. Thongvitokomarn S, Polchai N. Indocyanine green fluorescence versus blue dye or radioisotope regarding detection rate of sentinel lymph node biopsy and nodes removed in breast cancer: a systematic review and meta-analysis. *Asian Pac J Cancer Prev.* 2020;21:1187–1195.
55. Dayan JH, Dayan E, Smith ML. Reverse lymphatic mapping: a new technique for maximizing safety in vascularized lymph node transfer. *Plast Reconstr Surg.* 2015;135:277–285.
56. Chang EI, Chu CK, Hanson SE, et al. Comprehensive overview of available donor sites for vascularized lymph node transfer. *Plast Reconstr Surg Glob Open.* 2020;8:e2675.
57. Pan W-R. Distribution of lymphatics. In: Pan W-R, ed. *Atlas of Lymphatic Anatomy in the Head, Neck, Chest and Limbs.* Singapore: Springer Nature Singapore Pte Ltd.; 2017:125–236. Chap 3.
58. Scaglioni M, Suami H. Anatomy of the lymphatic system and the lymphosome concept with reference to lymphedema. *Semin Plast Surg.* 2018;37:5–11.
59. Koshima I, Narushima M, Mihara M, et al. Lymphadiposal flaps and lymphaticovenular anastomoses for severe leg edema: functional reconstruction for lymph drainage system. *J Reconstr Microsurg.* 2016;32:50–55.
60. Akita S, Yamaji Y, Tokumoto H, et al. Improvement of the efficacy of vascularized lymph node transfer for lower-extremity lymphedema via a prefabricated lympho-venous shunt through lymphaticovenular anastomosis between the efferent lymphatic vessel and small vein in the elevated vascularized lymph node. *Microsurgery.* 2018;38:270–277.